Global optimization of the Hydraulic-electromagnetic Energy-harvesting Shock Absorber for road vehicles with Human-knowledge-integrated Particle Swarm Optimization scheme

Zhou, Q.; Guo, Sijing; Xu, Lin; Guo, Xuexun; Williams, H.; Xu, H.; Yan, Fuwu

DOI:
10.1109/TMECH.2021.3055815

Document Version
Peer reviewed version

Citation for published version (Harvard):
Zhou, Q, Guo, S, Xu, L, Guo, X, Williams, H, Xu, H & Yan, F 2021, 'Global optimization of the Hydraulic-electromagnetic Energy-harvesting Shock Absorber for road vehicles with Human-knowledge-integrated Particle Swarm Optimization scheme', *IEEE/ASME Transactions on Mechatronics*, vol. 26, no. 3, 9343693, pp. 1225-1235. https://doi.org/10.1109/TMECH.2021.3055815

Global Optimization of the Hydraulic-electromagnetic Energy-harvesting Shock Absorber for Road Vehicles with Human-knowledge-integrated Particle Swarm Optimization Scheme

Quan Zhou, *Member, IEEE*, Sijing Guo*, Lin Xu, Xuexun Guo, Huw Williams, Hongming Xu*, and Fuwu Yan

***Abstract.* — This paper proposes a Human-knowledge-integrated Particle Swarm Optimization (Hi-PSO) scheme to globally optimize the design of the Hydraulic-electromagnetic Energy-harvesting Shock Absorber (HESA) for road vehicles. A newly developed k-fold swarm learning framework is the key to the Hi-PSO scheme, which runs k groups (folds) of individual local optimization (using a selected learning cycle), and validation (using the other k-1 testing cycles) with the concept of digital twin introduced into the design of the HESA. It aims to achieve the optimum energy recovery efficiency globally in both learning cycles and testing cycles. Within the learning framework, a nearest-neighborhood particle swarm learning algorithm is developed to incorporate human-knowledge (e.g., ISO standards) for local optimization so that the computational load can be reduced through downsizing of the learning spaces. Experiments have been conducted to evaluate the energy recovery and damping performance under both local conditions (duty cycles used for learning) and global conditions (six duty cycles covering the main equivalent amplitudes and frequencies of the suspension's operation). Compared with the conventional PSO algorithm, Hi-PSO is shown to be more robust by achieving a 5.17% higher mean value in 10 trials while achieving the same maximum energy efficiency. The global optimum result is obtained under 20 mm/1.5 Hz condition and achieves an average energy efficiency of 59.07%.**

***Index Terms*— Global optimization; Particle swarm optimization; K-fold swarm learning; Mechatronics in road mobility; Energy harvesting shock absorber; Digital twin.**

I. Introduction

GROWING concerns for air quality and the advent of zero-emission zones have prompted the automotive industry to seek low-cost carbon emission reduction solutions [1], [2]. Apart from powertrain electrification [3], [4], energy recovery technologies, e.g. kinetic energy recovery [5], [6], thermal energy recovery [7], [8], vibration energy recovery [9], [10], have been intensively researched to improve vehicles' energy efficiency.

In a passenger car, the dissipated vibration energy reaches 400W for the four shock absorbers [11]. If the dissipated energy can be regenerated into electricity with an energy recovery efficiency of 60% [12], the fuel economy can be improved by at least 2.5% [13]. In addition, an energy harvesting shock absorber can provide continuously variable damping for semi-active suspension control [14], [15]. Therefore, energy harvesting shock absorbers have been proposed to improve vehicle's energy efficiency, drivability, and ride comfort [16].

Generally, there are two main types of energy regenerative shock absorbers, the linear electromagnetic shock absorber (LEMSA) [14], [16] and the rotary electromagnetic shock absorber (REMSA) [17], [18]. LEMSA generates electricity with linear-moving coils in static magnetic fields [15]. However, LEMSA is inappropriate for vehicle applications because LEMSA with sufficient recovery power to meet the damping requirements is too large in size to be packaged in a road vehicle [19], [20]. REMSA generates electricity using low-cost rotary motors, and both mechanical [21], [22] and hydraulic rectifiers [23], [24] have been studied to convert reciprocating vibration into unidirectional rotation of the generator for REMSA. This reduces irregular oscillation and enhances the durability of the electricity generation systems. Hydraulic rectifiers have been shown to be more robust compared to mechanical rectifiers because they can bear the larger impact forces that are common in vehicle suspension. The hydraulic rectifier is also more flexible because it only needs the hydraulic cylinder to be installed in the suspension, while other components can be mounted on the chassis [23]. The hydraulic rectifier is also compatible with interconnected suspensions which can provide a favorable compromise between drivability and riding comfort [10]. The Hydraulic-electromagnetic Energy-harvesting Shock Absorber (HESA) is one of the REMSAs with a hydraulic rectifier, which has been proposed by the authors [24].

Theorical and proof-of-concept studies on HESA have been intensively conducted in recent years. Fang et al. conducted an experimental study on the damping and energy recovery characteristics of a HESA [25]. Zhang et al. analyzed the sensitivity of the design parameters to the damping and energy regeneration characteristics of a HESA [26]. Guo et al. developed a HESA model considering the hydraulic inertia that was shown to be accurate and robust with respect to experimental data [23]. Zhang et al. conducted a feasibility study on energy harvesting from a vehicle suspension with HESA [27]. Zhou et al. evaluated the damping and energy harvesting performance of HESA in an off-highway vehicle [28]. Mi et al. studied the feasibility of energy harvesting from railway vehicles using HESA [29]. Zou et al. analyzed the riding comfort and drivability of an interconnected suspension using HESA [30].

Only a few studies have focused on the optimization of HESA systems. Zheng et al. optimized the 8 design variables based on Design of Experiments (DoE) studies that compromised 16 groups of testing under 25 mm/1 Hz condition with different settings of the design variables [31]. The

Q. Zhou, S. Guo, L. Xu, X. Guo, H.M. Xu, and Fuwu Yan are with the School of Automotive Engineering, Wuhan University of Technology, Wuhan, 430070, China

Q. Zhou, Huw Williams, and H.M. Xu are with the Department of Mechanical Engineering, the University of Birmingham, Birmingham, B15 2TT, UK

* Corresponding author: S. Guo (sijingg@whut.edu.cn) and H.M. Xu (h.m.xu@bham.ac.uk)

optimization result can only be regarded as a local optimum because the 16 groups of tests cannot cover all the possible combinations of design parameters. Zou et al. implemented a Genetic Algorithm (GA) to determine the optimal design parameters of HESA for a vehicle running on a class D road surface [32]. Although GA is recognized as a global parameter searching algorithm, the result can still only be regarded as a local optimum because it is obtained under one single use case that cannot fully represent the real-world conditions.

Global optimization is a new key enabler to help the Hydraulic-electromagnetic Energy-harvesting Shock Absorber (HESA), which is a promising automotive mechatronic system, advance into real-world application. Efficient local optimization for the selected learning conditions (as challenge 1) and robust global optimization for both learning conditions and validation conditions (as challenge 2) are the two issues that must be addressed for global optimization of the HESA system as in other engineering systems.

For challenge 1, artificial intelligence has shown effective in enabling practical optimization in engineering. Meta-heuristic algorithms (e.g. Generic Algorithms [33], [34] and Particle Swarm Optimization (PSO) algorithms [35], [36]) have been proposed to conduct global searches in learning conditions, and are more computationally efficient than exhaustive searching. The PSO algorithm, which mimics the intelligence of birds flocking, is one of the most widely used AI-learning algorithms in automotive engineering. Mamun et al. determined the optimal component specification and control parameters of a vehicle using a PSO algorithm [37]. Zhang et al conducted transient diesel engine calibration with PSO [38]. Zhou et al proposed a cyber-physical vehicle control based on the PSO algorithm [39]. Transfer learning is an emerging technology that can accelerate AI learning processes based on prior knowledge of the objects. The approaches that enable knowledge transfer include transferring of characteristics [40], feature representations [41], model parameters [42], and relational knowledge [43]. There is a large amount of research into transfer learning for classification problems [44], but studies on incorporating human-knowledge into AI-learning procedures remain scarce.

For challenge 2, cross-validation is a statistical method that is used to estimate the skill of machine learning models to prevent overfitting in local learning [45]. It divides the source data into two datasets (the training dataset and the validation dataset) and implements several rounds of training and validation to obtain the global best solution that is robustly good in both training and validation sets. K-fold cross-validation is a widely used method for learning with labelled data [45]. Lv et al. implemented five-fold cross-validation in training a neuro-network for driver intention prediction [46]. Zuo et al developed a five-fold method for training a fuzzy model in solving regression problems [47]. Tivive used a ten-fold method to train a convolutional neuro-network for pattern recognition [48]. There is a lack of results on using K-fold cross-validation method for PSO-based design optimization of the HESA system.

To address the two challenges in global optimization of the main parameters of the HESA system, this paper proposes a Human-knowledge-integrated Particle Swarm Optimization (Hi-PSO) scheme. Experiments were conducted to evaluate energy recovery and damping performance. This work focuses on incorporating computational intelligence with the concept of digital twin introduced into the design of the HESA, which is conducted by providing two main contributions,

1) A new nearest-neighborhood particle swarm optimization algorithm is proposed for local optimization in the Hi-PSO scheme, which optimizes the integer design variables in the learning spaces that are downsized by human knowledge.
2) The k-fold swarm learning framework, which incorporates k-fold cross-validation with particle swarm optimization, is proposed for the Hi-PSO to ensure that the optimization result is globally robust with respect to varying conditions.

The rest of the paper is organized as follows: Section II develops the digital twin of the HESA, which is based on the first principle of the hydraulic system. The Human-knowledge-integrated Particle Swarm Optimization (Hi-PSO) scheme for design optimization of HESA is proposed in Section III. Experimental validations and evaluations are conducted in Section IV. Section V summarizes the conclusions.

II. Digital Twin of the Hydraulic-electromagnetic Energy Harvesting Shock Absorber (HESA)

The HESA prototype and schematic of the system are shown in **Fig. 1**. The HESA system works in parallel with a spring in a suspension, aiming to recover the vibration energy as electricity and mitigate the vibration in the vehicle suspension. The digital twin of the HESA is developed in the laboratory, which includes a HESA model and data interfaces that interact with artificial intelligence algorithm in the server computer. The HESA is modelled from a system level, including its hydraulic circuit and energy recovery unit. The energy recovery efficiency is defined as the optimization objective with the consideration of both hydraulic friction loss and energy conversion efficiency.

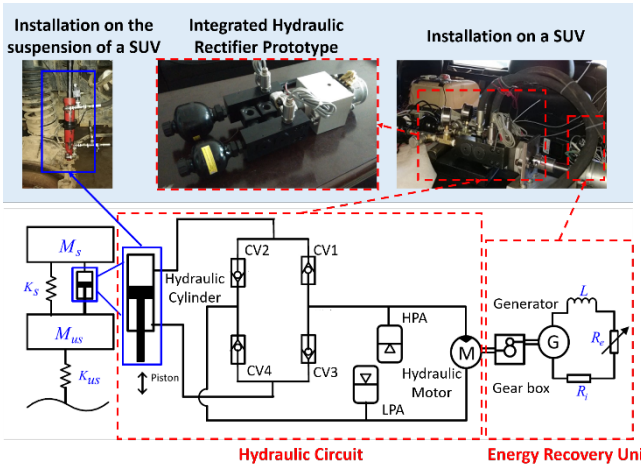

Fig. 1 The HESA prototype and the schematic of the HESA system

A. Hydraulic Circuit

The hydraulic circuit of the HESA includes a hydraulic cylinder, a rectifier composed of four check valves (CV1-4), a high-pressure accumulator (HPA), a low-pressure accumulator (LPA), and a hydraulic motor. The hydraulic cylinder replaces

the traditional shock absorber in a suspension, and the other hydraulic components can be integrated into a chassis-mounted assembly as in **Fig. 1**.

One key component in the HESA is the hydraulic rectifier, which converts the bi-directional vibration of the piston to a unidirectional rotation of the hydraulic motor to avoid the energy loss in the rotation-reversing process. When the piston of the hydraulic cylinder moves up, it pushes the fluid out of the hydraulic cylinder to the hydraulic motor through the CV1 and back to the hydraulic cylinder through CV4, and the motor rotates clockwise. When the piston moves downward, the fluid is pushed to the motor through the CV3 and back to the hydraulic cylinder through CV2, and the motor rotates clockwise as well.

The HPA and LPA are installed at the inlet and outlet of the hydraulic motor, respectively with the purpose to stabilize the fluid pressure at the inlet of the hydraulic motor and complement the fluid change in the hydraulic circuit. The pressure drop ΔP_m between the HPA and the LPA is

$$\Delta P_m(t) = \frac{P_{H1}\cdot {V_{H1}}^r}{(V_{H1}-V_h(t))^r} - \frac{P_{L1}\cdot {V_{L1}}^r}{(V_{L1}+V_h(t)-A_r(D)\cdot z_p(t))^r} \tag{1}$$

where P_{H1} and P_{L1} are the gas pressure of HP accumulator and LP accumulator when the HESA is initially installed in the vehicle, respectively; V_{H1} and V_{L1} are the initial gas volume of HPA and LPA, respectively; r represents the adiabatic index; $V_h(t)$ is the fluid volume change (based on initial state) in the high-pressure accumulator at time t; $A_r(D)$ is the area of the piston rod where D is the inner diameter of the cylinder; $z_p(t)$ is the piston displacement at time t.

Since fluid-charging is very fast, the pressure and volume of HP and LP accumulators can be calculated via polytropic process equations such that

$$\left.\begin{aligned} P_{H1} = P_i,\quad V_{H1} = V_{H0}\left(\frac{P_{H0}}{P_{H1}}\right)^{1/r} \\ P_{L1} = P_i,\quad V_{L1} = V_{L0}\left(\frac{P_{L0}}{P_{L1}}\right)^{1/r} \end{aligned}\right\} \tag{2}$$

where P_i is the pre-set initial environmental pressure in the hydraulic circuit, and P_{H0}, V_{H0}, P_{L0}, V_{L0} are the gas pressure and gas volume of the HP and LP accumulators at the free state.

The flow rate to the hydraulic motor Q_m is

$$Q_m = \left|Q_p\right| - \dot{V}_h \tag{3}$$

where Q_p and $\dot{V}_h$ respectively represent the flow rate from the hydraulic cylinder (driven by the piston) and the flow rate into (out of) the accumulator; the absolute value of $Q_p = \frac{\pi D^2}{4}\cdot v_p$ is due to the hydraulic rectifier, which converts the bidirectional flow to a unidirectional flow; D and v_p are the diameter and velocity of the cylinder piston.

B. Energy Recovery Unit

The energy recovery unit includes a hydraulic motor, an electric generator, and a gearbox connecting them. According to the Newton's law, the relationship between the torque of the hydraulic motor T_m and the electromotive torque of the generator T_{emf} yields

$$\left.\begin{aligned} T_m - n_g\cdot T_{emf} = J_g\cdot\dot{\omega}_g \\ T_m = \frac{\Delta P_m\cdot D_m}{2\pi}\cdot\eta_m \\ T_{emf} = \frac{U_{emf}}{R_i+R_{ex}}\cdot k_t \\ \omega_g = \frac{2\pi\cdot\eta_v\cdot n_g}{D_m}\cdot Q_m \end{aligned}\right\} \tag{4}$$

where n_g is the gear ratio of the gearbox; J_g is the inertia of the rotational components; ω_g is the rotation speed of the generator; ΔP_m and Q_m are the pressure drop and the flow rate across the hydraulic motor; D_m, η_m, and η_v are the displacement, the mechanical and volumetric efficiency of the hydraulic motor; k_t, R_i, R_{ex}, and U_{emf} are the torque constant, the internal resistance, the external resistance, and the back electromagnetic force of the generator; $U_{emf} = k_e\omega_g$, where k_e is the generator's speed constant and its value is equal to k_t.

The pressure drop across the hydraulic motor ΔP_m can be derived from equation (1)-(4) as

$$\Delta P_m(t) = \frac{4\pi^2\cdot {n_g}^2\cdot\eta_v}{{D_m}^2\cdot\eta_m}\cdot\left(J_g\cdot\dot{Q}_m(t) + \frac{k_t\cdot k_e\cdot Q_m(t)}{R_i+R_{ex}}\right) \tag{5}$$

C. Damping Force Excitation

The damping force can be calculated based on the pressure drop between the high-pressure chamber and the low-pressure chamber, namely the sum of the pressure drops across the hydraulic motor, ΔP_m, and the hydraulic pipeline, ΔP_f. Meanwhile, the hydraulic rectifier, which converts the bi-directional flow into a uni-directional flow, always forces ΔP_m and ΔP_f to have positive values. The damping force has the same direction as the moving direction of the cylinder. Hence, the damping force can be modelled by

$$F_d = (\Delta P_m + \Delta P_f)\cdot S\cdot \mathrm{sign}(v_p) \tag{6}$$

where $S = \frac{\pi D^2}{4}$ is the sectional area of the piston; $v_p = \dot{z}_p$ is the speed of the cylinder piston; $\mathrm{sign}(v_p)$ is the sign function of the piston speed v_p; and ΔP_f is the pressure drop in the hydraulic circuit due to the hydraulic friction such that [27]

$$\left.\begin{aligned} \Delta P_f = (a_1+a_2)\cdot {v_p}^2 + a_3\cdot v_p\cdot\mathrm{sign}(v_p) \\ a_1 = \lambda\cdot\rho\cdot\frac{l}{2d}\cdot\left(\frac{D}{d}\right)^4 \\ a_2 = 6\varsigma_i\cdot\left(\frac{D}{d}\right)^4 \\ a_3 = k_1\cdot\frac{\pi\cdot D^2}{2} \end{aligned}\right\} \tag{7}$$

where l and d are, respectively, the hose length and hose diameter; ρ is the fluid density; λ is the friction factor, which can be obtained by looking up the moody chart with known tube roughness and Reynolds number; ς_i is the local friction coefficient; and k_1 is a constant which equals to 3×10^8, given by the product brochure of the check valve.

D. Energy Recovery Efficiency

The energy recovery efficiency is defined by dividing the electric energy E_{ele} by the mechanical energy E_{mech} such that

$$\eta_r = \frac{E_{\mathrm{ele}}}{E_{\mathrm{mech}}} \tag{8}$$

The mechanical energy, which is absorbed by the HESA from vibration, is calculated by

$$E_{\text{mech}} = \int_{t_0}^{t_t} F_d(t)\, v_p(t) dt \tag{9}$$

where t_0 and t_t are the start time and stop time in a duty cycle; and $F_d(t)$ and $v_p(t)$ are the damping force and position velocity at time t.

The electricity generated from the HESA is calculated by

$$E_{\text{ele}} = \int_{t_0}^{t_t} \frac{U_{\text{emf}}(t)^2}{R_i + R_{ex}} dt \tag{10}$$

Based on Equations (1), (6-10), the energy efficiency can be written as a function of design parameters $\boldsymbol{X}$ and the duty cycle $\boldsymbol{C}$ such that

$$\eta_r = \text{HESA}(\boldsymbol{\chi}, \boldsymbol{C}) \tag{11}$$

where HESA(·) is the generic model that calculates the energy efficiency of the HESA; $\boldsymbol{\chi} = [D, D_m, n_g, k_t, R_i, R_{ex}, P_{H0}, V_{H0}]^T$ is a vector of design parameters; $\boldsymbol{C} = [Z, f]$ is a vector of duty cycle parameters; and Z and f are the displacement and frequency of the suspension.

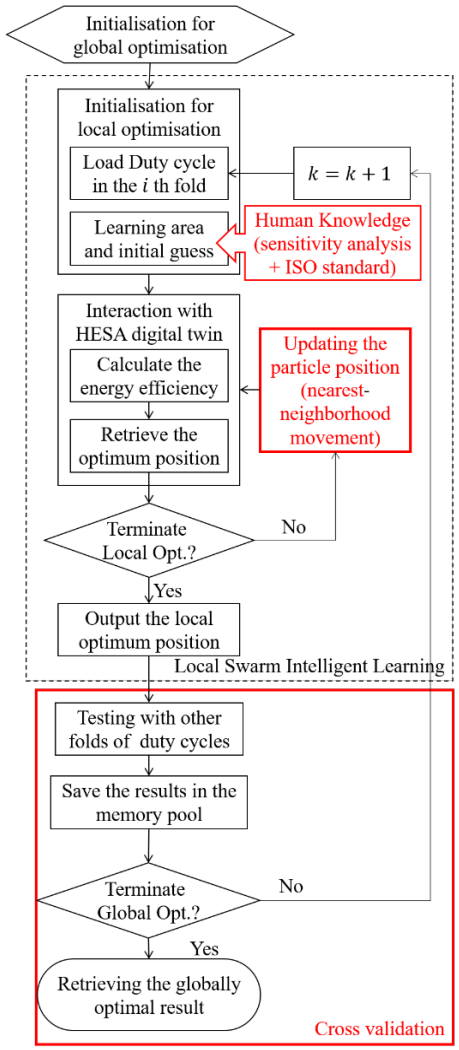

Fig. 2 The proposed Human-knowledge-integrated Particle Swarm Optimisation for the HESA

III. Human-knowledge-integrated Particle Swarm Optimization for the HESA

The proposed Human-knowledge-integrated Particle Swarm Optimization (Hi-PSO) is based on a K-fold swarm learning framework, as shown in **Fig. 2**, to achieve globally optimal design parameters for the HESA. Human knowledge, including sensitivity analysis results and ISO standards, are incorporated in the swarm intelligence learning process to reduce the search space for the optima with a mixed-integer particle swarm optimization algorithm.

A. K-fold Swarm Learning Framework

One of the design targets of the proposed Hi-PSO for global optimisation of the HESA is to allow the best system to be adapted to most of the damper stroke (amplitude)/ frequency duty cycles. The cross-validation under the selected six duty cycles aims to provide compliant and comprehensive evaluations because every local optimisation result (obtained in one learning cycle) is validated in other five testing cycles (it can be regarded as evaluations on combined cycles of five duty cycles). The proposed k-fold swarm learning implements k-fold cross-validation in the process of retrieving the optimal parameter vector $\boldsymbol{X}^*$ as shown in **Fig. 3**, where the duty cycles labelled with 'L' are used for learning, and the duty cycles labelled with 'T' are used for testing. The involvement of testing cycles with larger amplitude/frequency ranges (five times larger than the learning cycles) provides complementary environments to comprehensively evaluate local optimization results so that the global optimal design can be attained adaptively to real-world situations. Following the authors' recent work on acquiring the power spectrum of the suspension vibration on road test with the Fourier transform [49], which suggested the dominant frequencies for the HESA are under 5Hz, six duty cycles are defined to cover most of the common amplitude/frequency ranges of vehicle suspensions in Table I.

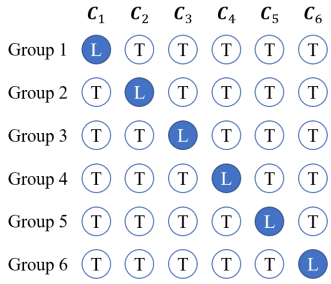

Fig. 3 Data partition in the k-fold swarm learning

Table I Duty cycles for HESA optimization

Duty cycles	$\boldsymbol{C}_1$	$\boldsymbol{C}_2$	$\boldsymbol{C}_3$	$\boldsymbol{C}_4$	$\boldsymbol{C}_5$	$\boldsymbol{C}_6$
Amplitude Z (mm)	20	20	20	50	10	2
Frequency f (Hz)	0.5	1.5	2	0.5	5	10

A rotational learning-testing cross validation process is conducted by repeating the following three procedures for six groups of optimizations,

1) Local optimization is conducted individually under one of the defined duty cycles, i.e., $\boldsymbol{C}_k = [Z_k, f_k]^T$ $(k = 1,2,\ldots,6)$, to obtain the locally optimal result $\boldsymbol{X}_k^*$.

2) The HESA with the parameter vector $\boldsymbol{X}_k^*$ is tested under other duty cycles apart from $\boldsymbol{C}_k$, e.g., $\boldsymbol{C}_1, \boldsymbol{C}_2, \dots \boldsymbol{C}_{k-1}, \boldsymbol{C}_{k+1}, \dots \boldsymbol{C}_6$ $(2 < k < 4)$, to obtain the energy recovery efficiencies and damping characteristics.
3) The result $\boldsymbol{X}_k^*$, including energy recovery efficiencies and damping characteristics, is saved in a memory pool.

The global optimization terminated when all six groups of optimizations are complete. The global optimal result is then selected by considering energy recovery efficiency and damping performance, which will be discussed in Section IV.

B. Local Swarm Intelligence Learning

Local swarm intelligence learning algorithm is developed based on particle swarm optimization (a software that mimics swarming insects) to solve the local optimization problem under a given duty cycle $\boldsymbol{C}_k$. The local optimization problem can be formulated mathematically as

$$\boldsymbol{X}_k^* = \arg\max \eta_r = \mathrm{HESA}(\boldsymbol{X}, \boldsymbol{C}_k) \quad \text{s.t.} \begin{cases} \boldsymbol{X} \in \mathbb{X} \\ \boldsymbol{C}_k = [Z_k, f_k]^T \in \{\boldsymbol{C}_1, \boldsymbol{C}_2, \dots, \boldsymbol{C}_6\} \\ z_p = Z_k \cdot \sin(2\pi \cdot f_k) \\ max \frac{F_d(t)}{v_p(t)} \le c^+ \\ \text{other constrains defined in HESA}(\cdot) \end{cases} \tag{12}$$

where $\boldsymbol{X}_k^*$ is the locally optimal result at the k-th group of optimizations; $\mathbb{X}$ is the learning space where the swarm intelligence retrieves the optimization result; z_p is the displacement of the vehicle suspension modelled by a sine function with the amplitude Z_k and frequency f_k defined in the duty cycle $\boldsymbol{C}_k$; and c^+ is the upper boundary of the damping ratio defined by dividing the damping force $F_d(t)$ with piston speed $v_d(t)$. $c^+ = 2.4 \times 10^4$ is chosen for passenger vehicles.

1) Downsizing of the learning space with human knowledge

The proposed Hi-PSO scheme transfers human-knowledge in hydraulic system design for selection of the number of design variables and their candidate value. This is a way of feature space-based transfer learning [41]. The learning space $\mathbb{X}$ is a multiple dimensional space. Both the number of design variables and the candidate values for each design variable determine the size of the learning space $\mathbb{X}$ that affects the learning efficiency and computational effort.

The HESA is modelled with the parameters of $D, D_m, n_g, k_t, R_i, R_{ex}, P_{H0}$, and V_{H0}. In this paper, the number of design variables were reduced based on human knowledge of sensitivity analysis and an understanding of the HESA systems. A sensitivity study on the hydraulic system of the HESA suggested that the pressure P_{H0} and volume V_{H0} of the accumulator has very low impact on the suspension performance [26]. Torque constant k_t and internal resistance R_i can be regarded as two coupled motor parameters if the motor-generator is chosen from off-the-shelf products to reduce cost. The external resistance R_{ex} is a controllable variable, and it is better optimized via design of the control system after the physical components of the HESA have been confirmed. Therefore, D, D_m, n_g, k_t, are selected to be optimized with the Hi-PSO. This reduced the number of variables that needs to be optimized from 8 to 4.

Conventional PSO retrieves the optimal values of the design variables in a space that is restricted by the lower and upper boundary of each design variable. Although the number of candidate values for the design variables can be reduced by using a larger step length Δx in the search space $\{x^-, x^- + \Delta x, x^- + 2 \cdot \Delta x, \dots, x^+\}$, this may miss the truly optimal result if an improper Δx is chosen.

The specification of standard hydraulic components, e.g., diameters of the hydraulic cylinder, are specified by ISO standards. In this study, the learning space is through replacing the continuously varying learning spaces by sets of the available component specifications which are defined in ISO 3320:2013 and ISO 8426:2008 for hydraulic cylinders and hydraulic motors, respectively. The using of the specification in the ISO standards also allows the prototyping of the HESA with less cost and time. The learning space $\mathbb{X} = [\mathbb{D}, \mathbb{D}_m, \mathbb{m}_g, \mathbb{k}_t]^T$ is redefined by involving ISO standards (human knowledge), where $\mathbb{D}, \mathbb{D}_m, \mathbb{m}_g$, and $\mathbb{k}_t$ are vectors of the candidate values for D, D_m, n_g, and k_t as in Table II.

Table II Downsized Learning Area with Human Knowledge

Design variable	Learning space	Candidate value vector
D	$\mathbb{D}$	[25, 32, 40, 50, 63, 80]
D_m	$\mathbb{D}_m$	[8, 10, 12.5, 14, 16, 18, 20, 25, 28, 31.5]
n_g	$\mathbb{m}_g$	[2, 2.1, 2.2, 2.3, …, 9.8, 9.9,10]
k_t	$\mathbb{k}_t$	[0.16, 0.165, 0.170, …, 0.235, 0.24]

2) Nearest-neighborhood Particle Swarm Optimization Algorithm

The local swarm learning is based on the particle swarm optimization (PSO) algorithm, which defines the particle positions at each iteration by the value of the design variables

$$\left.\begin{matrix} \boldsymbol{x}_{i,j} = [D, D_m, n_g, k_t]^T \\ i = 0,1,2, \dots, n;\ j = 1,2,.., p \end{matrix}\right\} \tag{13}$$

where $\boldsymbol{x}_{i,j}$ is the 'position' of the j^{th} 'particle' at i^{th} iteration; n is the maximum number of iterations, which is used to terminate the iterations; and p is the population of the particles, which defines the capability of global search in each iteration via computing agents.

A matrix of particle positions $[\boldsymbol{x}_{i,1}, \boldsymbol{x}_{i,2}, \boldsymbol{x}_{i,3}, \dots, \boldsymbol{x}_{i,p}] \in \mathbb{X}^{\boldsymbol{p}}$ supplies the inputs to the HESA twin in MATLAB/Simulink for each iteration. The HESA twin simulates p cases in parallel and outputs the energy recovery efficiency η_r and a timeseries of the damping force $\boldsymbol{F}_d = [F_d(t_0), F_d(t_0 + \Delta t), \dots, F_d(t_t)]$, where Δt is the sampling time.

The local best position in the i th iteration, $\boldsymbol{lb}_{i,*}$, is defined by a column of the trial matrix, $[\boldsymbol{x}_{i,1}, \boldsymbol{x}_{i,2}, \dots, \boldsymbol{x}_{i,p}]$ that satisfies

$$\eta_r\left(\boldsymbol{lb}_{i,*}\right) \le \eta_r\left(\boldsymbol{x}_{i,j}\right) \tag{14}$$

where $\eta_r\left(\boldsymbol{x}_{i,j}\right)$ is the energy recovery efficiency that achieved with the design parameter values in each $\boldsymbol{x}_{i,j}$ value; $i = 1,2, \dots, n;\ j = 1,2,.., p$.

The global best position in the i th iteration, $\boldsymbol{gb}_{i,*}$, is defined by a column of the local best matrix, $[\boldsymbol{lb}_{1,*}, \boldsymbol{lb}_{2,*}, \dots, \boldsymbol{lb}_{i,*}]$, that satisfies

$$\eta_r\left(\boldsymbol{gb}_{i,*}\right) \le \eta_r\left(\boldsymbol{lb}_{i,*}\right) \tag{15}$$

Conventional PSO updates its particle position by

$$\left.\begin{aligned} \boldsymbol{x}_{i+1,j} &= \boldsymbol{x}_{i,j} + \boldsymbol{v}_{i+1,j} \\ \boldsymbol{v}_{i+1,j} &= \boldsymbol{v}_{i,j} + c_1 \cdot \mathrm{Rnd}(0,1) \cdot \left(\boldsymbol{lb}_{i,*} - \boldsymbol{x}_{i,j}\right) \\ &\quad + c_2 \cdot \mathrm{Rnd}(0,1) \cdot \left(\boldsymbol{gb}_{i,*} - \boldsymbol{x}_{i,j}\right) \end{aligned}\right\} \tag{16}$$

where $\boldsymbol{v}_{i,j}$ is the velocity that the j th particle changes its position at the i th iteration; Rnd(0,1) is a random number generator that generates a vector of random numbers between 0 and 1 at each iteration; and c_1 and c_2 are factors that scales the attraction from local best $\boldsymbol{lb}_{i,*}$ and global best $\boldsymbol{gb}_{i,*}$.

Equation (16) updates the particle positions based on the assumption that the candidate design parameter is continuously varying between the lower and upper boundary. It cannot deal with the learning space as described in Table II. Therefore, a nearest-neighborhood position update mechanism was developed for the PSO algorithm which regulates the position calculated in equation (16) by finding the nearest candidate value $\boldsymbol{x'}_{i+1,j} = [D', D'_m, n'_g, k'_t]^T \in \mathbb{X}$ that satisfies

$$\left.\begin{aligned} \|D' - D\| &\le \|\mathbb{D}^{\mathrm{n1}} - D\| && \mathrm{n1} = 1,2,\dots,6 \\ \|D'_m - D_m\| &\le \left\|\mathbb{D}_{\mathrm{m}}{}^{\mathrm{n2}} - D_m\right\| && \mathrm{n2} = 1,2,\dots,10 \\ \left\|n'_g - n_g\right\| &\le \left\|\mathbb{m}_{\mathrm{g}}{}^{\mathrm{n3}} - n_g\right\| && \mathrm{n3} = 1,2,\dots,81 \\ \|k'_t - k_t\| &\le \left\|\mathbb{k}_{\mathrm{t}}{}^{\mathrm{n4}} - k_t\right\| && \mathrm{n4} = 1,2,\dots,17 \end{aligned}\right\} \tag{17}$$

where $\mathbb{D}^{\mathrm{n1}}$, $\mathbb{D}_{\mathrm{m}}{}^{\mathrm{n2}}$, $\mathbb{m}_{\mathrm{g}}{}^{\mathrm{n3}}$, and $\mathbb{k}_{\mathrm{t}}{}^{\mathrm{n4}}$ are elements in the candidate vectors within the learning space, $\mathbb{D} = [\mathbb{D}^1, \mathbb{D}^2, \dots, \mathbb{D}^6]$, $\mathbb{D}_m = [\mathbb{D}_{\mathrm{m}}{}^1, \mathbb{D}_{\mathrm{m}}{}^2, \dots, \mathbb{D}_{\mathrm{m}}{}^{10}]$, $\mathbb{m}_g = [\mathbb{m}_{\mathrm{g}}{}^1, \mathbb{m}_{\mathrm{g}}{}^2, \dots, \mathbb{m}_{\mathrm{g}}{}^{81}]$, and $\mathbb{k}_t = [\mathbb{k}_{\mathrm{t}}{}^1, \mathbb{k}_{\mathrm{t}}{}^2, \dots, \mathbb{k}_{\mathrm{t}}{}^{17}]$, respectively.

The iteration ends when the termination condition ($i = n$) is met, and the algorithm will extract the global best at the last iteration as the local optimization result.

IV. Experimental Studies

The experimental study was conducted in four stages. In the first stage, the HESA twin was validated by testing a physical HESA prototype. The energy recovery performance at local conditions and global conditions were investigated based on a software-in-the-loop testing platform at stages two and three respectively to examine the effectiveness of the optimization results. The damping characteristics were evaluated at the fourth stage to study the feasibility of implementation of the optimized HESA on the suspension of road vehicles.

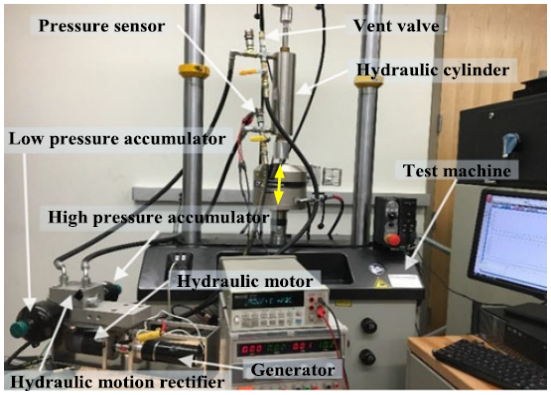

Fig. 4 Lab test setup

A. Experimental Validation of the Digital Twin of HESA

To validate the digital twin of HESA, lab tests and numerical simulations were both conducted. The lab test setup is shown in **Fig.4**. A HESA prototype was tested in an Instron 8801 machine that provides displacement excitation for the hydraulic cylinder. The damping force, generated power, displacement, and velocity were measured under excitations of 1 Hz/10 mm and 1 Hz/15 mm. The specifications of the HESA prototype are shown in Table III.

Table III Specifications of the HESA prototype

Parameter	Value	Nomenclature
D	0.0635m/2.5inch	Piston diameter
ν	$2.1 \times 10^{-6} m^2/s$	Fluid kinematic viscosity
l	2 m	Pipe length
d	0.016 m/ (5/8 inch)	Pipe diameter
P_{H0}	500,000 Pa	Initial gas pressure of HPA
V_{H0}	$0.16\times 10^{-3}\ m^3$	Initial gas volume of HPA
P_{L0}	200,000 Pa	Initial gas pressure of LPA
V_{L0}	$0.32\times 10^{-3}\ m^3$	Initial gas volume of LPA
P_i	500,000 Pa	Initial environmental pressure
D_m	$28 \times 10^{-6}\ m^3/r$	Hydraulic motor displacement
J_g	$560 \times 10^{-7}\ kg \cdot m^2$	Inertia of the generator
R_i	3.9Ω	Resistance of the generator
k_e	0.242Vs/rad	Generator voltage constant
k_t	0.242Nm/A	Generator torque constant
n_g	4.3	Gear ratio of the gear box

The force and power characteristics of the digital twin of HESA were simulated by MATALB 2019a on a PC with an Intel Core i7-8700 CPU and 16GB RAM. Simulation results obtained under the excitations of 10 mm/1 Hz and 15 mm/ 1 Hz are compared with the testing results in **Fig.5**. The HESA twin that was built by from first principles analysis of hydraulic systems is shown to predict the performance of the physical HESA prototype. In addition, a higher peak and a lower peak can be observed in the power curves, which is due to the piston rod in the cylinder inducing different flow rates from the cylinder in the extension stroke and the compression stroke. The HESA twin built in this paper was therefore used for optimization with Hi-PSO.

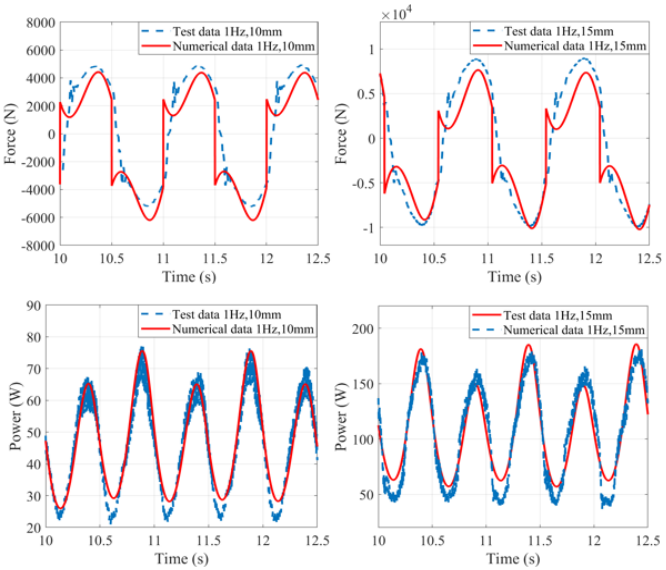

Fig. 5 Testing results vs simulation with the HESA digital twin

B. Local Energy Recovery Performance

Local energy recovery performance were evaluated by monitoring the maximum energy efficiency that can be achieved by the local swarm intelligence learning in the six given duty cycles (with the specifications listed in Table I). To investigate the local swarm learning performance, the optimized design parameters and energy recovery efficiency (under the 20 mm/1.5 Hz condition) obtained with the Hi-PSO in 10 individual trials are firstly compared with the results obtained by conventional PSO algorithm in **Fig.6**. In each subplot, the red and blue edge bars show the frequency that the values attained in the 10 trials by Hi-PSO and PSO, respectively. The red and blue solid lines illustrate the estimated normal distribution (based on the data from 10 trials) for Hi-PSO (fit) and PSO (fit), respectively. The best settings for each design parameter that achieves the maximum energy recovery efficiency are shown by the green solid line (Opt.). The algorithm performs better if it has higher frequency (probability) to achieve the optimal solution.

In general, the proposed Hi-PSO outperforms conventional PSO by having greater opportunity to achieve the maximum energy recovery efficiency as shown in **Fig.6 e)**. The proposed Hi-PSO has higher probability of accessing the optimal setting for cylinder diameter D and motor displacement D_m in both real measurement and normal distribution estimation. Hi-PSO and conventional PSO have the same probability to attain optimal gear ratio n_g. Although both Hi-PSO and PSO can obtain the same optimal solution under the condition of 20 mm/1.5 Hz, it should be noticed that conventional PSO may find better solutions than Hi-PSO because human-knowledge may prevent access to the solution that has better performance

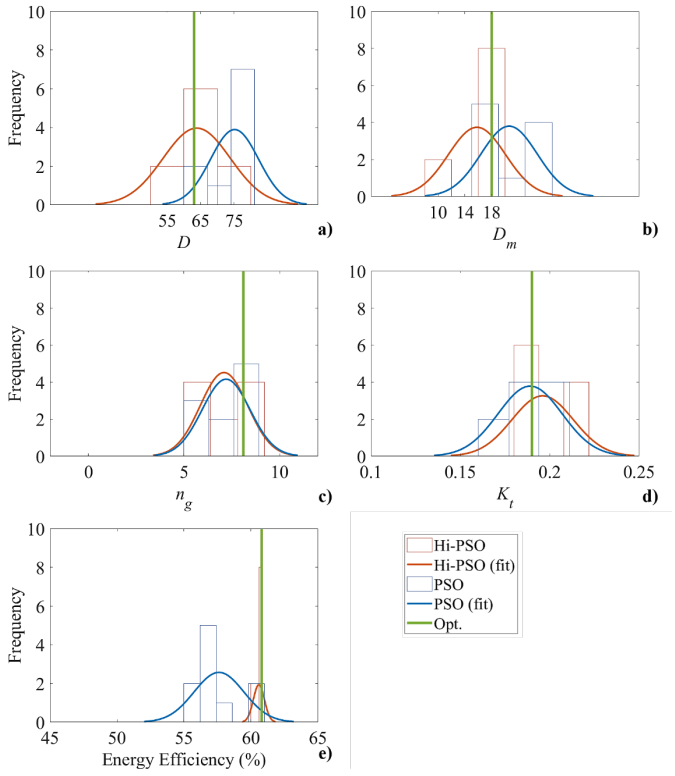

Fig. 6 Optimization results in 10 trials: a) cylinder diameter D; b) hydraulic motor displacement D_m; c) gear ratio of gearbox n_g; d) torque constant k_t; e) energy efficiency.

in some scenarios. However, conventional PSO has a much lower ability to access better solution than the Hi-PSO (as shown in Fig.6) because the larger learning space increases the computational effort and reduces the probability of accessing the optima. Therefore, the Hi-PSO has been shown effective to provide solutions for rapid prototyping of the HESA system.

The local optimal design parameters for the HESA and its energy recovery efficiency under the six duty cycles ($\boldsymbol{C_1} - \boldsymbol{C_6}$) are then compared in Table IV. As results of the local swarm learning, the HESA can have at least 57.57% energy efficiency with different settings for its design parameters. The maximum energy recovery efficiency that can be achieved locally is 62.09% with the design parameters optimized under duty cycle $\boldsymbol{C_6}$. When looking at the locally optimal settings for each design parameter, the design parameters have at least three different values as the local optimal settings. The diameter D has 3 different settings; the motor displacement D_m has 4 different settings; the gear ratio n_g has 5 different settings; and the motor torque constant k_t has 4 different settings. In real engineering practice, the design parameters should be fixed for production, therefore design parameters obtained in each local learning should not only achieve the maximum energy recovery efficiency locally under the scenario for learning, but also be robust with respect to other scenarios.

Table IV Local optimization results and the maximum energy recovery efficiency in learning cycles

Duty cycles	$\boldsymbol{C_1}$	$\boldsymbol{C_2}$	$\boldsymbol{C_3}$	$\boldsymbol{C_4}$	$\boldsymbol{C_5}$	$\boldsymbol{C_6}$
D	80mm	63mm	50mm	50mm	50mm	**80mm**
D_m	14cc	18cc	10cc	12.5cc	12.5cc	**10cc**
n_g	6.1	8.1	7.1	5.6	10	**10**
k_t	0.2	0.19	0.23	0.2	0.18	**0.19**
η_r	0.5797	0.6080	0.6140	0.5757	0.6194	**0.6209**

C. Global Energy Recovery Performance

To test the robustness of the local optimization results, global energy recovery performance was evaluated with six groups of tests as shown in **Fig.7**. The locally optimal design parameters obtained in $\boldsymbol{C_1}$ to $\boldsymbol{C_6}$ are tested under other duty cycles in the respective testing groups, e.g., in Group 1, the locally optimal design parameters obtain in $\boldsymbol{C_1}$ is tested under duty cycle $\boldsymbol{C_2}$ to $\boldsymbol{C_6}$ at testing group 1. The energy efficiencies obtained under

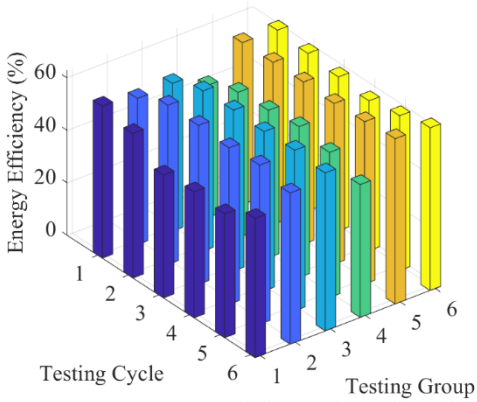

Fig. 7 Energy recovery efficiency that achieved under the six testing groups

learning duty cycle and testing duty cycles for each group are shown in the bars with same color. In general, the locally optimal design parameters achieve different energy efficiency values under different testing duty cycles. Sometimes, similar energy recovery efficiency is achieved in the testing duty cycle and the learning duty cycles. In some cases, the energy recovery performance is very poor, e.g., in testing group 1 and 4. The energy recovery efficiencies achieved in each testing duty cycle for each testing group are displayed in Table V.

Table V Energy efficiency performance in testing duty cycles

Duty cycles	C_1	C_2	C_3	C_4	C_5	C_6
Group 1	-	0.5580	0.5640	0.5045	0.6172	0.6134
Group 2	0.5512	-	0.6112	0.5546	0.6183	0.6011
Group 3	0.4688	0.6073	-	0.5622	0.6189	0.5872
Group 4	0.4804	0.5976	0.6078	-	0.6128	0.5718
Group 5	0.4725	0.6075	0.6129	0.5537	-	0.5910
Group 6	0.5309	0.5769	0.6023	0.5065	0.6304	-

From a global performance perspective, the locally optimal design parameters obtained under $\boldsymbol{C_1}$, $\boldsymbol{C_2}$ and $\boldsymbol{C_6}$ are shown to be more adaptive, achieving the energy efficiency with values of at least 50%, whereas the results obtained under $\boldsymbol{C_3}$-$\boldsymbol{C_5}$ show less adaptiveness in some duty cycles where the energy efficiency they can achieve is less than 50%. From the statistical summary of the results in each testing group, as in Table VI, the locally optimal design parameter obtained under $\boldsymbol{C_2}$ (i.e., 20 mm/1.5 Hz) is shown to be the most robust by achieving the highest mean value and lowest variation of energy efficiency in the testing duty cycles.

Table VI Statistic summary of the results in each testing groups

Groups	*1*	***2***	*3*	*4*	*5*	*6*
μ	0.5714	**0.5873**	0.5689	0.5741	0.5675	0.5694
σ	0.0463	**0.0320**	0.0600	0.0547	0.0579	0.0507

D. Global Damping Force Performance

Damping characteristics are important for the HESA to absorb the vibration. The damping coefficient F_d/v_p was limited in local swarm learning as in Section III.B, and the force-displacement performance were further evaluated under both learning and testing conditions to validate the design results. The force-displacement loops, which use their area to quantify the mechanical energy that can be absorbed by the HESA, are shown in **Fig.8**. Each subplot of **Fig.8** summarizes the force-displacement performance of the HESA that is locally optimised under $\boldsymbol{C_1}$ to $\boldsymbol{C_6}$, respectively. As an example, **Fig.8** a) presents the force-displacement performance of the HESA that is locally optimized under $\boldsymbol{C_1}$. In each subplot of **Fig.8**, the force-displacement loops under $\boldsymbol{C_1}$-$\boldsymbol{C_6}$ are shown in dark blue, yellow, green, red, purple, and light blue.

For the HESA with local optimal design parameters obtained under $\boldsymbol{C_1}$ and $\boldsymbol{C_6}$, it can be seen that the damping forces vary greatly under the same duty cycle, indicating that the locally optimized parameters in $\boldsymbol{C_1}$-$\boldsymbol{C_6}$ provides various damping property and fits for different types of vehicle. By considering the global performance in both energy recovery efficiency and damping characteristics, the HESA with the local optimal design parameters obtained under $\boldsymbol{C_2}$ is recognized as the global optimization result.

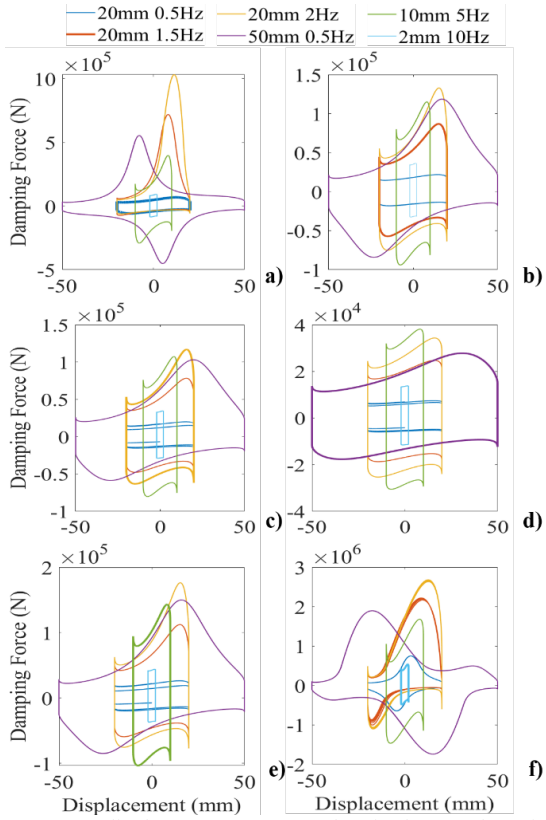

Fig. 8 Force-displacement Loops under six duty cycles with the HESA optimized under: a) 20mm/0.5Hz cycle ($\boldsymbol{C_1}$); b) 20mm/1.5Hz cycle ($\boldsymbol{C_2}$); c) 20mm/2.0Hz cycle ($\boldsymbol{C_3}$); d) 50mm/0.5 Hz cycle ($\boldsymbol{C_4}$); e) 10mm/5.0Hz cycle ($\boldsymbol{C_5}$); f) 2mm/10.0 Hz cycle ($\boldsymbol{C_6}$).

By comparing the damping performance with the energy recovery efficiency, a very interesting phenomenon can be observed, i.e., the damping performance varies more significantly than the energy efficiency for different local optimal designs. This is because the local swarm learning is a single objective (to maximize energy efficiency) optimization with constraints (e.g., damping coefficient range), and it retrieves the best design parameters which can achieve the maximum energy efficiency (as in Table IV). This will result in several designs that have less differences in energy efficiency but with more significant differences in damping forces (e.g., the local optima in $\boldsymbol{C_5}$ and $\boldsymbol{C_6}$). Therefore, it is very important to conduct global optimization with the proposed Hi-PSO scheme to confirm the feasibility of the design.

V. Conclusions

This paper proposed a Human-knowledge-integrated Particle Swarm Optimization (Hi-PSO) scheme to achieve global optimization of the design parameters of the HESA for a road vehicle. A digital twin of the HESA has been developed with testing validations of a HESA prototype. An experimental study has been conducted to evaluate the optimized HESA in terms of both energy recovery efficiency and damping characteristics. The conclusions drawn from the investigation are:

- The proposed Hi-PSO is effective in local swarm learning. It can achieve 5.17% higher energy efficiency compared to the results obtained by using conventional PSO in 10 individual tests under 20mm/1.5Hz duty cycle ($\boldsymbol{C}_2$).
- The local optimal design parameters obtained under $\boldsymbol{C}_2$ can be recognized as the global optimization result. They can achieve an average energy efficiency of 59.07% in the testing duty cycles, performing at least 2.2% better than the benchmark obtained by other methods.
- The damping force provided by the HESA with global optimization, i.e., the optimal setting obtained in $\boldsymbol{C}_2$, is proved applicable to isolate the vibration in a vehicle suspension. Additionally, the optimal setting obtained in C1-C6 presents different damping properties, which suit for different vehicles.

In the next stage, a prototype using an upgraded HESA with the global optimal design parameters will be manufactured and installed on a vehicle, in order to further research the active suspension control with artificial intelligence technology.

ACKNOWLEDGEMENT

This work was funded by National Natural Science Foundation of China (51905394), Ministry of Education of China under 111-project (B17034), and Hubei Natural Science Foundation of China (2019CFB202). The authors are also grateful to the support from Hubei Key Laboratory of Advanced Technology for Automotive Components, Hubei Collaborative Innovation Centre for Automotive Components Technology.

REFERENCE

[1] S. Tsiakmakis *et al.*, "From lab-to-road & vice-versa: Using a simulation-based approach for predicting real-world CO 2 emissions," *Energy*, vol. 169, pp. 1153–1165, 2019.

[2] C. Wang, H. Xu, J. M. Herreros, J. Wang, and R. Cracknell, "Impact of fuel and injection system on particle emissions from a GDI engine," *Appl. Energy*, vol. 132, no. 2014, pp. 178–191, 2014.

[3] C. Lv, J. Zhang, Y. Li, and Y. Yuan, "Mechanism analysis and evaluation methodology of regenerative braking contribution to energy efficiency improvement of electrified vehicles," *Energy Convers. Manag.*, vol. 92, pp. 469–482, 2015.

[4] Q. Zhou, X. Guo, G. Tan, X. Shen, Y. Ye, and Z. Wang, "Parameter Analysis on Torque Stabilization for the Eddy Current Brake: A Developed Model, Simulation, and Sensitive Analysis," *Math. Probl. Eng.*, vol. 2015, pp. 1–10, 2015.

[5] K. Kiddee, W. Keyoonwong, and W. Khan-Ngern, "An HSC/battery energy storage system-based regenerative braking system control mechanism for battery electric vehicles," *IEEJ Trans. Electr. Electron. Eng.*, vol. 14, no. 3, pp. 457–466, 2019.

[6] Q. Zhou, G. Tan, X. Guo, Z. Fang, and B. Gong, "Relationship between Braking Force and Pedal Force of a Pedal Controlled Parallelized Energy-Recuperation Retarder System," *SAE Tech. Pap. 2014-01-1783*, no. January 2013, 2014.

[7] X. Shen, G. Tan, Q. Zhou, Z. Yang, and M. Hua, "The Organic Medium Physical State Analysis for Engine Exhaust Thermal Recovery," *SAE Tech. Pap.*, vol. 2015-April, no. April, 2015.

[8] T. Y. Kim, J. Kwak, and B. wook Kim, "Application of compact thermoelectric generator to hybrid electric vehicle engine operating under real vehicle operating conditions," *Energy Convers. Manag.*, vol. 201, no. October, p. 112150, 2019.

[9] X. He *et al.*, "The applications of energy regeneration and conversion technologies based on hydraulic transmission systems: A review," *Energy Convers. Manag.*, vol. 205, no. August 2019, p. 112413, 2020.

[10] S. Guo, Z. Chen, X. Guo, Q. Zhou, and J. Zhang, "Vehicle Interconnected Suspension System based on Hydraulic Electromagnetic Energy Harvest: Design, Modeling and Simulation Tests," *SAE Tech. Pap. 2014-01-2299*, 2014.

[11] L. Zuo and P.-S. Zhang, "Energy Harvesting, Ride Comfort, and Road Handling of Regenerative Vehicle Suspensions," *J. Vib. Acoust.*, vol. 135, no. 1, Feb. 2013.

[12] Z. Li, L. Zuo, J. Kuang, and G. Luhrs, "Energy-harvesting shock absorber with a mechanical motion rectifier," *Smart Mater. Struct.*, vol. 22, no. 2, 2013.

[13] D. KARNOPP, "Permanent Magnet Linear Motors Used as Variable Mechanical Dampers for Vehicle Suspensions," *Veh. Syst. Dyn.*, vol. 18, no. 4, pp. 187–200, Jan. 1989.

[14] X. Tang, T. Lin, and L. Zuo, "Design and optimization of a tubular linear electromagnetic vibration energy harvester," *IEEE/ASME Trans. Mechatronics*, vol. 19, no. 2, pp. 615–622, 2014.

[15] Y. SUDA and T. SHIIBA, "A New Hybrid Suspension System with Active Control and Energy Regeneration," *Veh. Syst. Dyn.*, vol. 25, no. sup1, pp. 641–654, Jan. 1996.

[16] I. L. Cassidy, J. T. Scruggs, S. Behrens, and H. P. Gavin, "Design and experimental characterization of an electromagnetic transducer for large-scale vibratory energy harvesting applications," *J. Intell. Mater. Syst. Struct.*, vol. 22, no. 17, pp. 2009–2024, 2011.

[17] A. Maravandi and M. Moallem, "Regenerative shock absorber using a two-leg motion conversion mechanism," *IEEE/ASME Trans. Mechatronics*, vol. 20, no. 6, pp. 2853–2861, 2015.

[18] Z. Li, L. Zuo, G. Luhrs, L. Lin, and Y. X. Qin, "Electromagnetic Energy-Harvesting Shock Absorbers: Design, Modeling, and Road Tests," *IEEE Trans. Veh. Technol.*, vol. 62, no. 3, pp. 1065–1074, 2013.

[19] A. Gupta, J. A. Jendrzejczyk, T. M. Mulcahy, and J. R. Hull, "Design of electromagnetic shock absorbers," *Int. J. Mech. Mater. Des.*, vol. 3, no. 3, pp. 285–291, 2006.

[20] K. Singal and R. Rajamani, "Zero-Energy Active Suspension System for Automobiles With Adaptive Sky-Hook Damping," *J. Vib. Acoust.*, vol. 135, no. 1, Feb. 2013.

[21] L. Bowen, J. Vinolas, J. L. Olazagoitia, and J. Echavarri Otero, "An Innovative Energy Harvesting Shock Absorber System Using Cable Transmission," *IEEE/ASME Trans. Mechatronics*, vol. 24, no. 2, pp. 689–699, 2019.

[22] Y. Liu, L. Xu, and L. Zuo, "Mechanical-Motion-Rectifier-Based Energy Harvester Using a Ball-Screw Mechanism," *IEEE/ASME Trans. Mechatronics*, vol. 22, no. 5, pp. 1933–1943, 2017.

[23] S. Guo, L. Xu, Y. Liu, X. Guo, and L. Zuo, "Modeling and experiments of a hydraulic electromagnetic energy-harvesting shock absorber," *IEEE/ASME Trans. Mechatronics*, vol. 22, no. 6, pp. 2684–2694, 2017.

[24] S. Guo, Y. Liu, L. Xu, X. Guo, and L. Zuo, "Performance evaluation and parameter sensitivity of energy-harvesting shock absorbers on different vehicles," *Veh. Syst. Dyn.*, vol. 54, no. 7, pp. 918–942, 2016.

[25] Z. Fang, X. Guo, L. Xu, and H. Zhang, "Experimental study of damping and energy regeneration characteristics of a hydraulic electromagnetic shock absorber," *Adv. Mech. Eng.*, vol. 2013, 2013.

[26] H. Zhang, X. Guo, L. Xu, S. Hu, and Z. Fang, "Parameters analysis of hydraulic-electrical energy regenerative absorber on suspension performance," *Adv. Mech. Eng.*, vol. 2014, 2014.

[27] Y. Zhang, X. Zhang, M. Zhan, K. Guo, F. Zhao, and Z. Liu, "Study on a novel hydraulic pumping regenerative suspension for vehicles," *J. Franklin Inst.*, vol. 352, no. 2, pp. 485–499, 2015.

[28] Q. Zhou, X. Guo, L. Xu, G. Wang, and J. Zhang, "Simulation based Evaluation of the Electro-Hydraulic Energy-Harvesting Suspension (EHEHS) for Off-Highway Vehicles," *SAE Tech. Pap.*, vol. 2015-April, no. April, 2015.

[29] J. Mi, L. Xu, S. Guo, L. Meng, and M. A. A. Abdelkareem, "Energy harvesting potential comparison study of a novel railway vehicle bogie system with the hydraulic-electromagnetic energy-regenerative shock absorber," *2017 Jt. Rail Conf. JRC 2017*, 2017.

[30] J. Zou, X. Guo, M. A. A. Abdelkareem, L. Xu, and J. Zhang, "Modelling and ride analysis of a hydraulic interconnected suspension based on the hydraulic energy regenerative shock absorbers," *Mech. Syst. Signal Process.*, vol. 127, pp. 345–369, 2019.

[31] P. Zheng, R. Wang, J. Gao, and X. Zhang, "Parameter Optimisation of Power Regeneration on the Hydraulic Electric Regenerative Shock Absorber System," *Shock Vib.*, vol. 2019, 2019.

[32] J. Zou, X. Guo, L. Xu, G. Tan, C. Zhang, and J. Zhang, "Design,

Modeling, and Analysis of a Novel Hydraulic Energy-Regenerative Shock Absorber for Vehicle Suspension," *Shock Vib.*, vol. 2017, 2017.
[33] S. Guo, M. Dooner, J. Wang, H. Xu, and G. Lu, "Adaptive Engine Optimisation Using NSGA-II and MODA Based on a Sub-Structured Artificial Neural Network," no. September, pp. 7–8, 2017.
[34] H. Ma, Z. Li, M. Tayarani, G. Lu, H. Xu, and X. Yao, "Computational Intelligence Non-model-based Calibration Approach for Internal Combustion Engines," *J. Dyn. Syst. Meas. Control*, vol. 140, no. April, pp. 1–9, 2017.
[35] Q. Zhou *et al.*, "Intelligent sizing of a series hybrid electric power-train system based on Chaos-enhanced accelerated particle swarm optimization," *Appl. Energy*, vol. 189, pp. 588–601, 2017.
[36] Q. Zhou *et al.*, "Modified Particle Swarm Optimization with Chaotic Attraction Strategy for Modular Design of Hybrid Powertrains," *IEEE Trans. Transp. Electrif.*, 2020.
[37] A. Al Mamun, Z. Liu, D. M. Rizzo, and S. Onori, "An integrated design and control optimization framework for hybrid military vehicle using lithium-ion battery and supercapacitor as energy storage devices," *IEEE Trans. Transp. Electrif.*, vol. 5, no. 1, pp. 239–251, 2019.
[38] Y. Zhang, Q. Zhou, Z. Li, J. Li, and H. Xu, "Intelligent transient calibration of a dual-loop EGR diesel engine using chaos-enhanced accelerated particle swarm optimization algorithm," *Proc. Inst. Mech. Eng. Part D J. Automob. Eng.*, 2018.
[39] Q. Zhou *et al.*, "Cyber-Physical Energy-Saving Control for Hybrid Aircraft-Towing Tractor based on Online Swarm Intelligent Programming," *IEEE Trans. Ind. Informatics*, vol. 14, no. 9, pp. 4149–4158, 2018.
[40] X.-F. Liu *et al.*, "Neural Network-Based Information Transfer for Dynamic Optimization," *IEEE Trans. Neural Networks Learn. Syst.*, vol. 31, no. 5, pp. 1–14, 2019.
[41] H. Zuo, G. Zhang, V. Behbood, and J. Lu, "Feature Spaces-based Transfer Learning," pp. 1000–1005, 2015.
[42] L. Duan, I. W. Tsang, and D. Xu, "Domain transfer multiple kernel learning," *IEEE Trans. Pattern Anal. Mach. Intell.*, vol. 34, no. 3, pp. 465–479, 2012.
[43] D. Wang, Y. Li, Y. Lin, and Y. Zhuang, "Relational knowledge transfer for zero-shot learning," *30th AAAI Conf. Artif. Intell. AAAI 2016*, pp. 2145–2151, 2016.
[44] Z. Q. Zhao, P. Zheng, S. T. Xu, and X. Wu, "Object Detection with Deep Learning: A Review," *IEEE Trans. Neural Networks Learn. Syst.*, vol. 30, no. 11, pp. 3212–3232, 2019.
[45] G. James, D. Witten, T. Hastie, and R. Tibshirani, *An Introduction to Statistical Learning*. Springer, 2013.
[46] C. Lv *et al.*, "Hybrid-Learning-Based Classification and Quantitative Inference of Driver Braking Intensity of an Electrified Vehicle," *IEEE Trans. Veh. Technol.*, vol. 67, no. 7, pp. 5718–5729, 2018.
[47] H. Zuo, G. Zhang, W. Pedrycz, V. Behbood, and J. Lu, "Fuzzy Regression Transfer Learning in Takagi-Sugeno Fuzzy Models," *IEEE Trans. Fuzzy Syst.*, vol. 25, no. 6, pp. 1795–1807, 2017.
[48] F. H. C. Tivive and A. Bouzerdoum, "Efficient training algorithms for a class of shunting inhibitory convolutional neural networks," *IEEE Trans. Neural Networks*, vol. 16, no. 3, pp. 541–556, 2005.
[49] J. Mi, L. Xu, S. Guo, M. A. A. Abdelkareem, L. Meng, and L. Zuo, "The Dimension Match and Paramters Setting of the Hydraulic Motor for the Hydraulic-Electromagnetic Energy-Regenerative Shock Absorber," in *Proceedings of the ASME 2017 International Design Engineering Technical Conferences and Computers and Information in Engineering Conference*, 2017, pp. 1–9.

Quan Zhou (M'17) received BEng and MEng in vehicle engineering from Wuhan University of Technology, in 2012 and 2015, respectively. He received the Ph.D. in mechanical engineering from the University of Birmingham (UoB) in 2019. He is currently a Research Fellow and leads the Connected and Autonomous Systems for Electrified Vehicles (CASE-V) Research at UoB. His research interests include artificial intelligence and their application in vehicular systems. He received a visiting scholar award from Tsinghua University, in 2019.

Sijing Guo received her Ph.D. degree in vehicle engineering from Wuhan University of Technology, Wuhan, China, in 2018. She did scientific research as a visiting student at Virginia Tech, Blacksburg, VA, USA, from 2014 to 2016. She is currently a lecturer in Wuhan University of Technology. Her research interest includes vehicle dynamics and control, energy harvesting, and mechatronics design. Her research is supported by NSFC and industry.

Lin Xu received his Ph.D. degree in vehicle engineering from Wuhan University of technology, Wuhan, China, in 2011. He is currently an associate professor in Wuhan University of Technology. His research interest includes suspension dynamics, energy harvesting, mechatronics design. He is the original contributor who has proposed the hydro-electric energy-harvesting shock absorber (HESA) and has authored 16 papers in this field.

Xuexun Guo received his B.S. degree in mechanical engineering from Huazhong University of Science and Technology, Wuhan, China, in 1982, and Ph.D degree in mechanical engineering from Beijing Institute of Technology, Beijing, China, in 1995. He is a full professor at Wuhan University of Technology since 2001. Xuexun Guo's research interest includes automobile design, driveline system simulation and testing.

Huw Williams is an honorary professor at the UoB and the director of DEEPPOWER Innovation Ltd. He is a mathematician with over 20 years' experience in the automotive industry; he graduated from the University of Oxford in 1978 with a mathematics degree and went on to take a PhD in theoretical mechanics at the University of East Anglia. Huw joined Jaguar Land Rover (JLR) in 1986 and then become a Senior Engineering Specialist in JLR.

Hongming Xu received PhD from Imperial College London in 1995. He is a Professor of Energy and Automotive Engineering at the University of Birmingham and Head of Vehicle and Engine Technology Research Centre. He is also a visiting professor at Wuhan University of Technology. Prof Xu has six years of industrial experience with Jaguar Land Rover. He has over 400 journal and conference publications on advanced powertrain systems. He is a Fellow of SAE and IMechE.

Fuwu Yan received his B.S., M.S., and PhD degrees in internal combustion engines from Wuhan University of Technology, in 1989, 1992, and 2002, respectively. Prof Yan is currently a full professor and head of the School of Automotive Engineering at Wuhan University of Technology. He authored more than 100 journal/conference papers and more than 10 patents. His research interests include automobile powertrain design, powertrain dynamics and control.